Synthesis of a Next-Generation Taxoid by Rapid Methylation Amenable for ^{11}C-Labeling

Joshua D. Seitz,[†] Tao Wang,[†] Jacob G. Vineberg,[†] Tadashi Honda,[†,‡] and Iwao Ojima[†,‡]*

[†]Department of Chemistry, Stony Brook University - State University of New York, Stony Brook, NY 11794-3400

[‡]Institute of Chemical Biology and Drug Discovery, Stony Brook University - State University of New York, Stony Brook, NY 11794-3400

*Corresponding author: Iwao.ojima@stonybrook.edu

Table of Contents

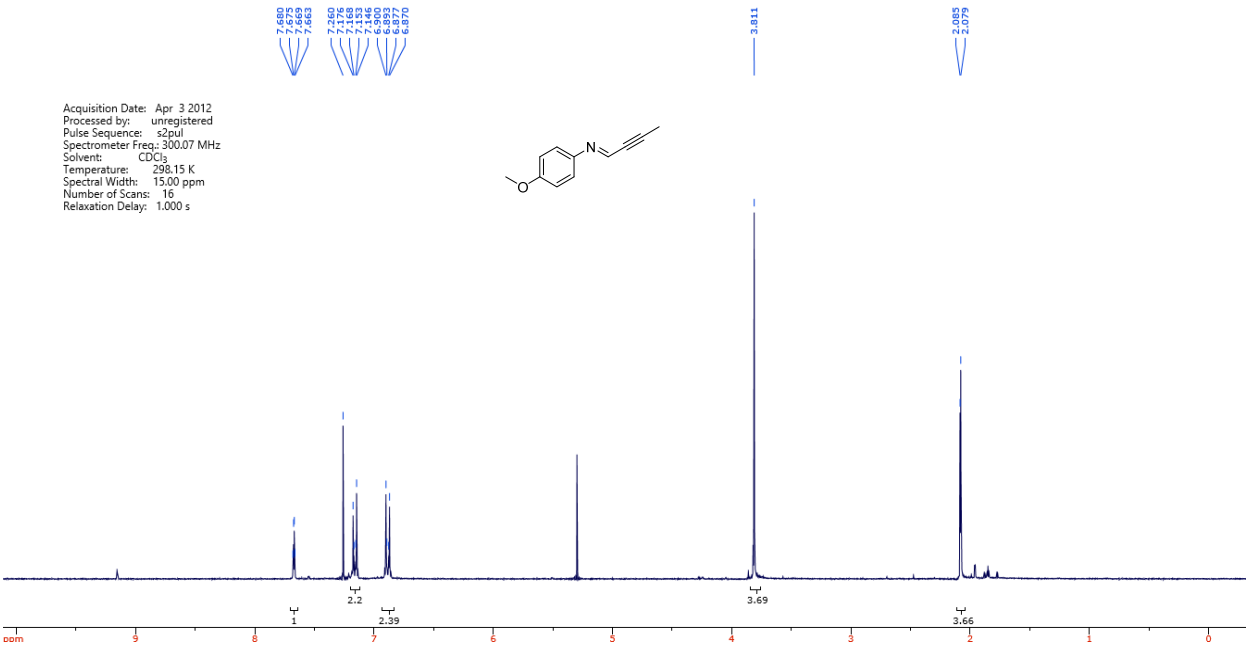

Figure S1. ^{1}H NMR spectrum of **6**

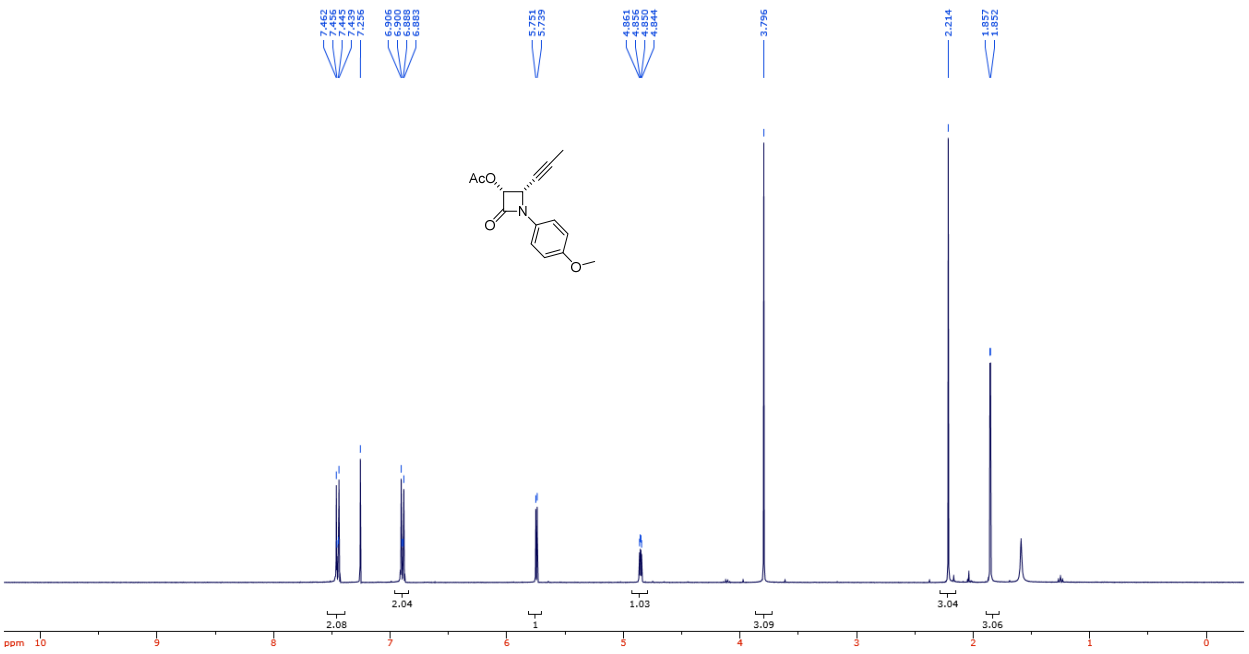

Figure S2. ^{1}H NMR spectrum of (±)**-7**

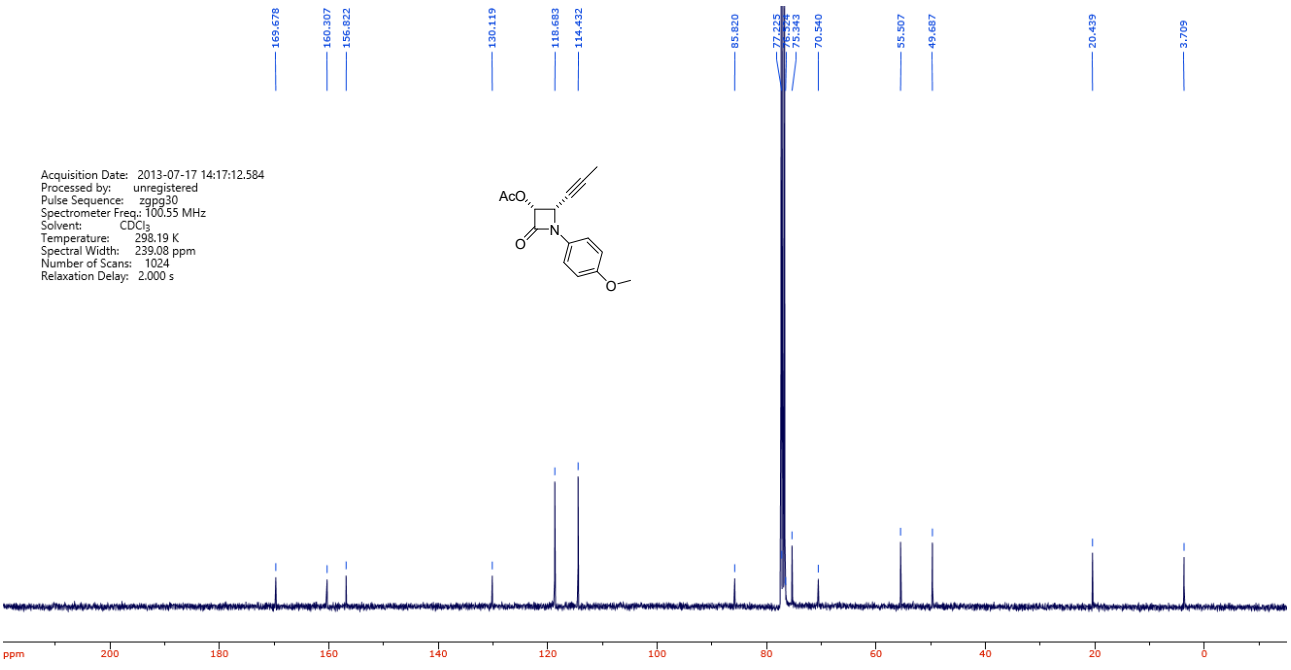

Figure S3. ^{13}C NMR spectrum of (±)**-7**

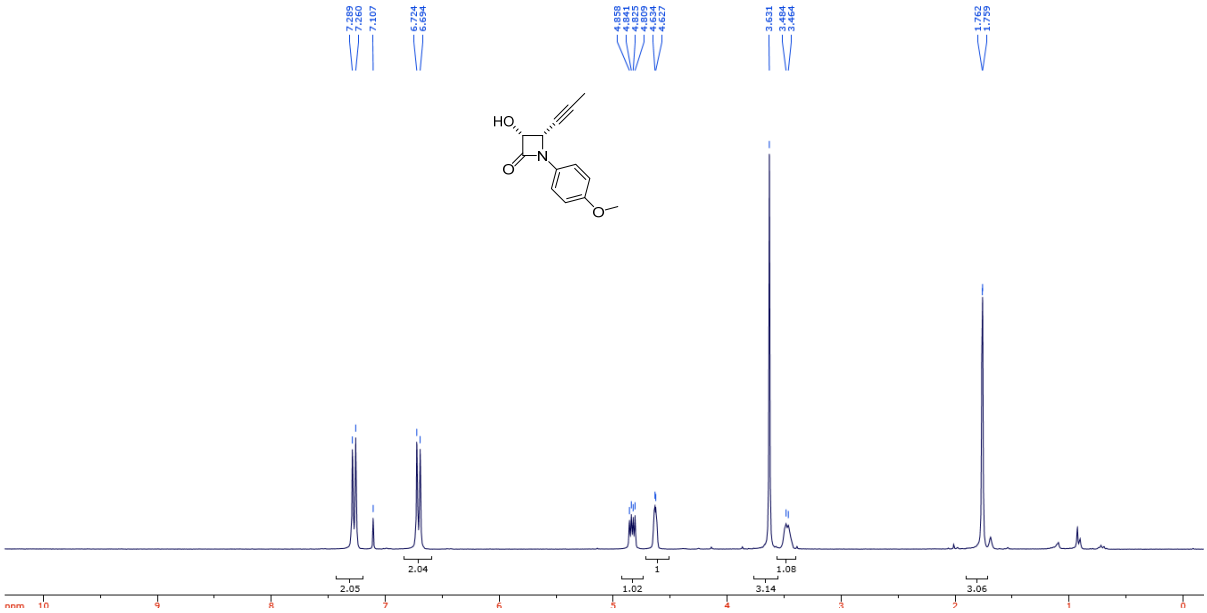

Figure S4. ^{1}H NMR Spectrum of (±)**-8**

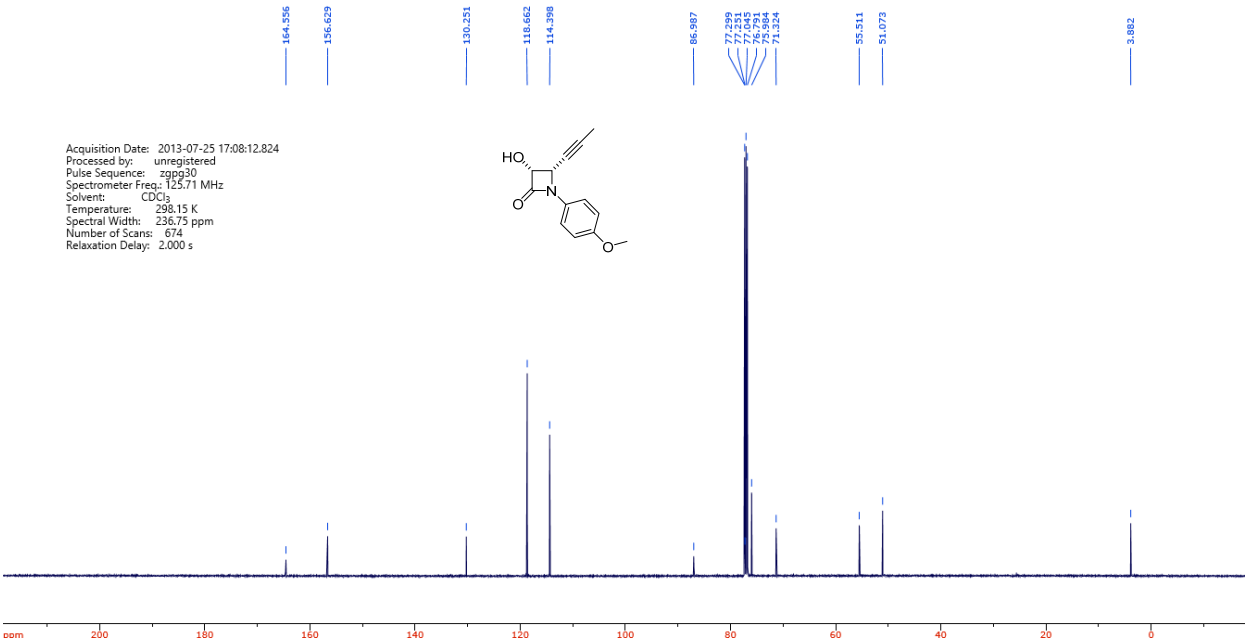

Figure S5. ^{13}C NMR spectrum of (±)**-8**

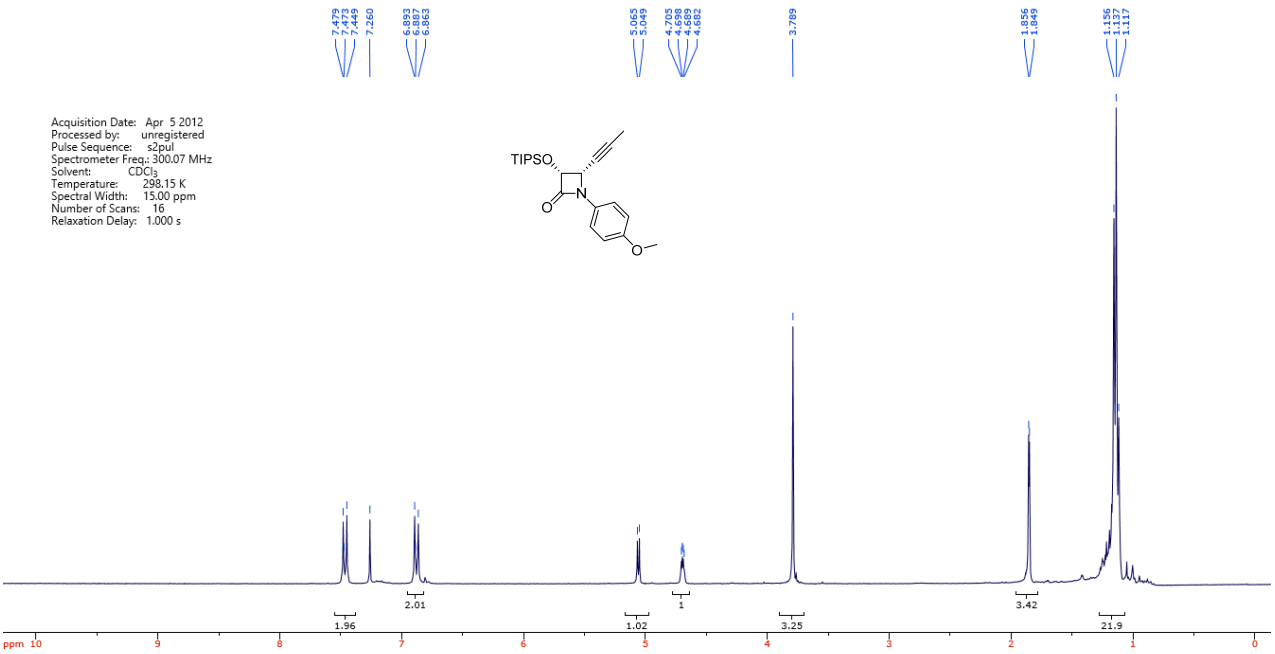

Figure S6. ^{1}H NMR spectrum of (+)**-9**

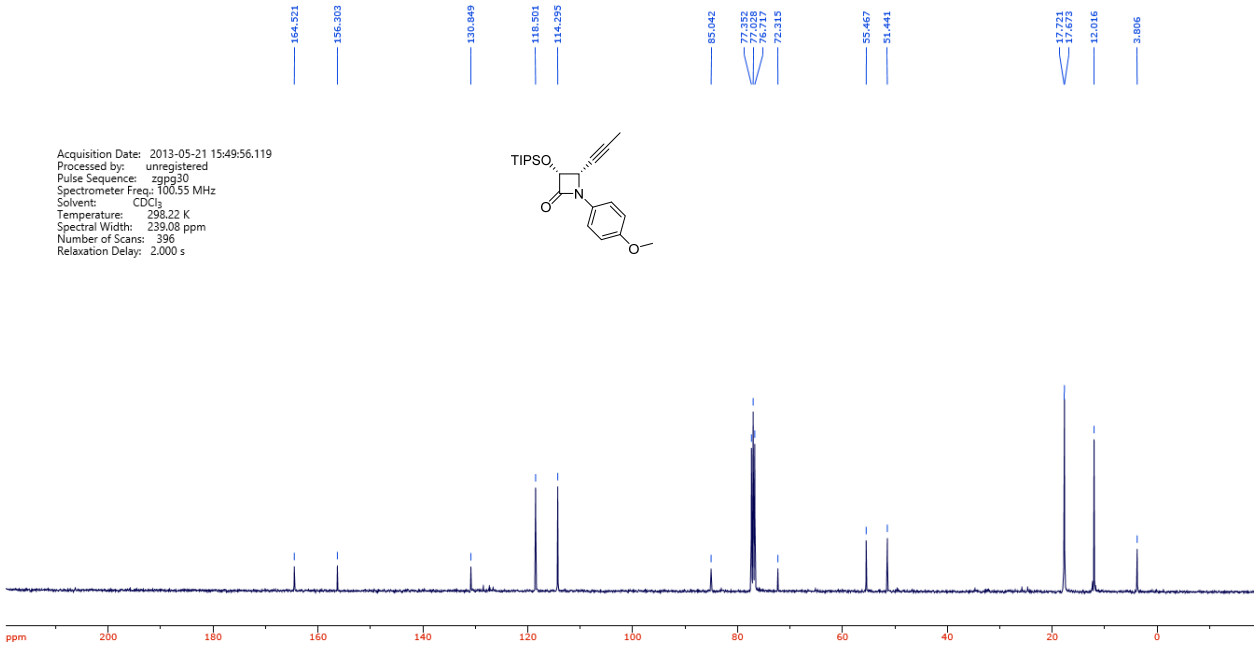

Figure S7. ^{13}C NMR spectrum of (+)**-9**

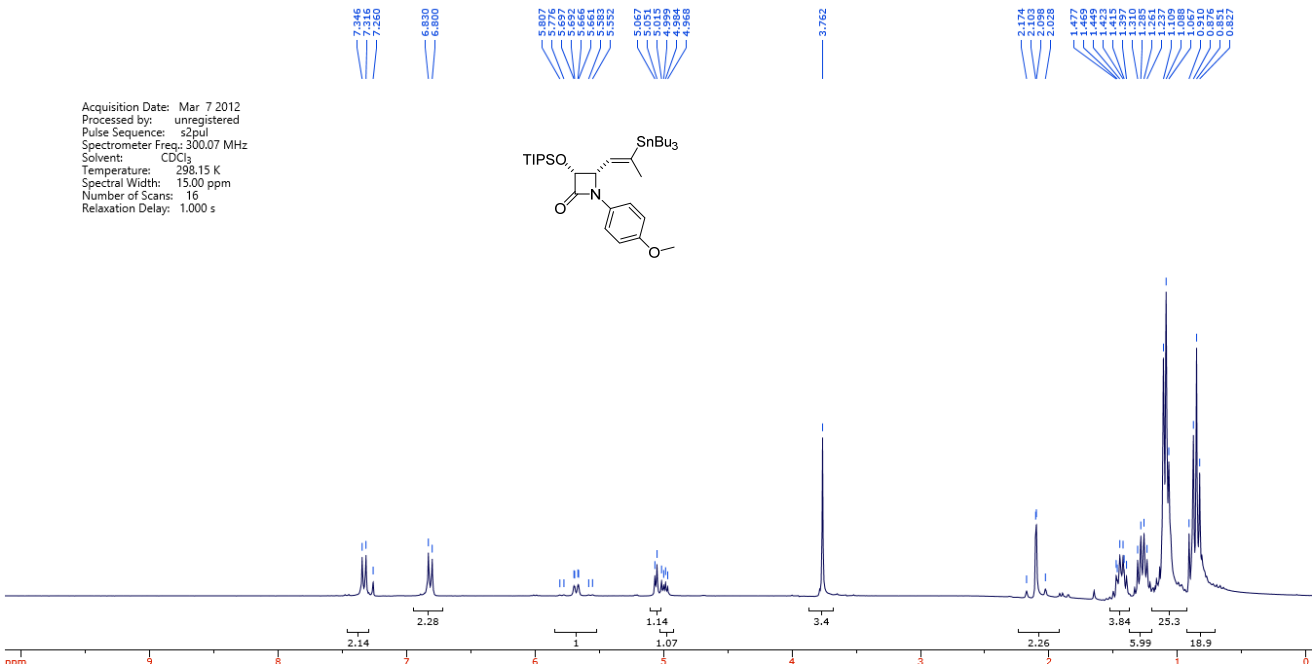

Figure S8. ^{1}H NMR spectrum of (±)**-10**

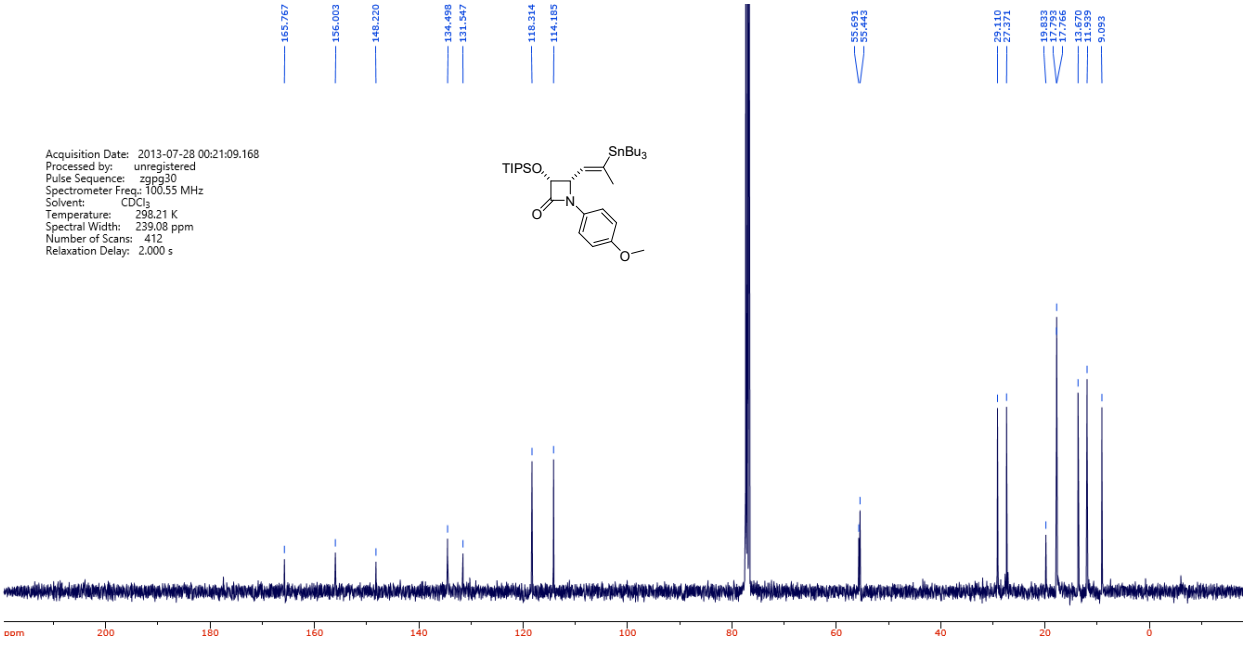

Figure S9. ^{13}C NMR spectrum of (±)**-10**

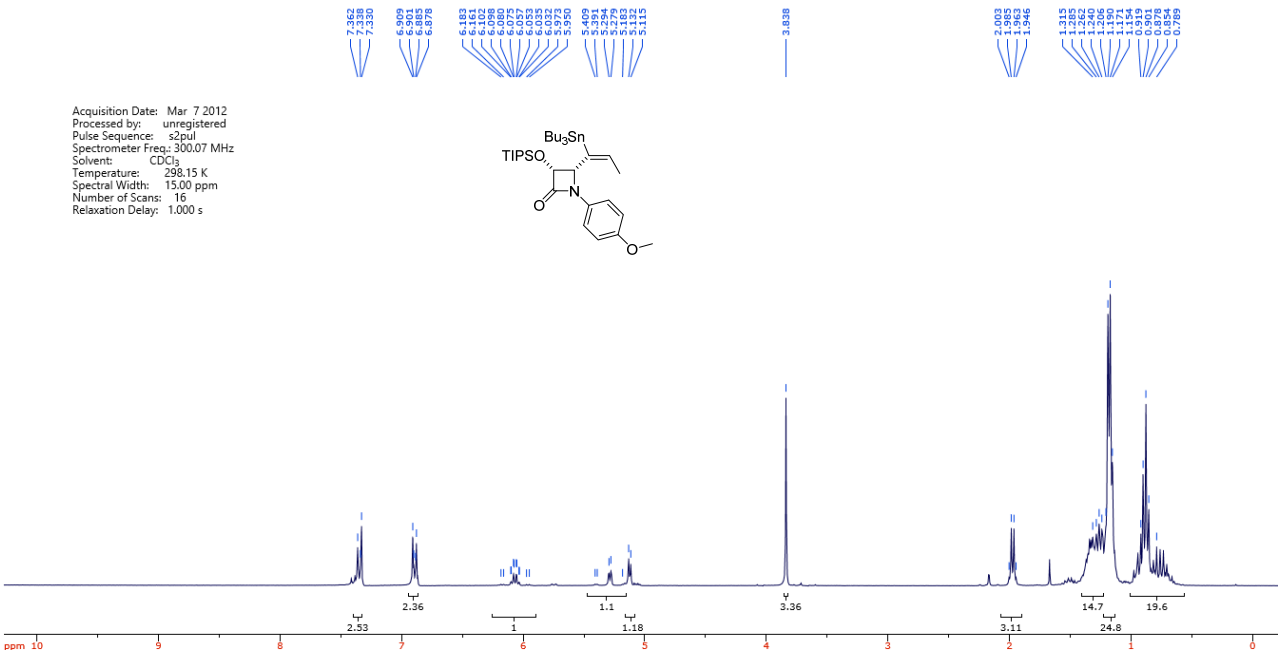

Figure S10. ^{1}H NMR spectrum of (±)**-11**

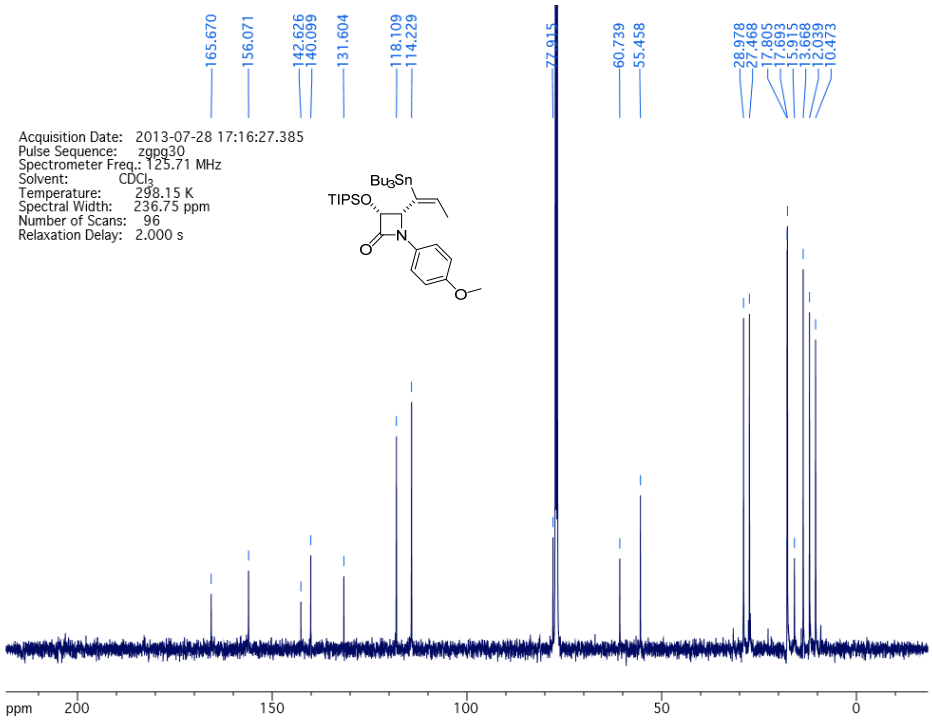

Figure S11. ^{13}C NMR spectrum of (±)**-11**

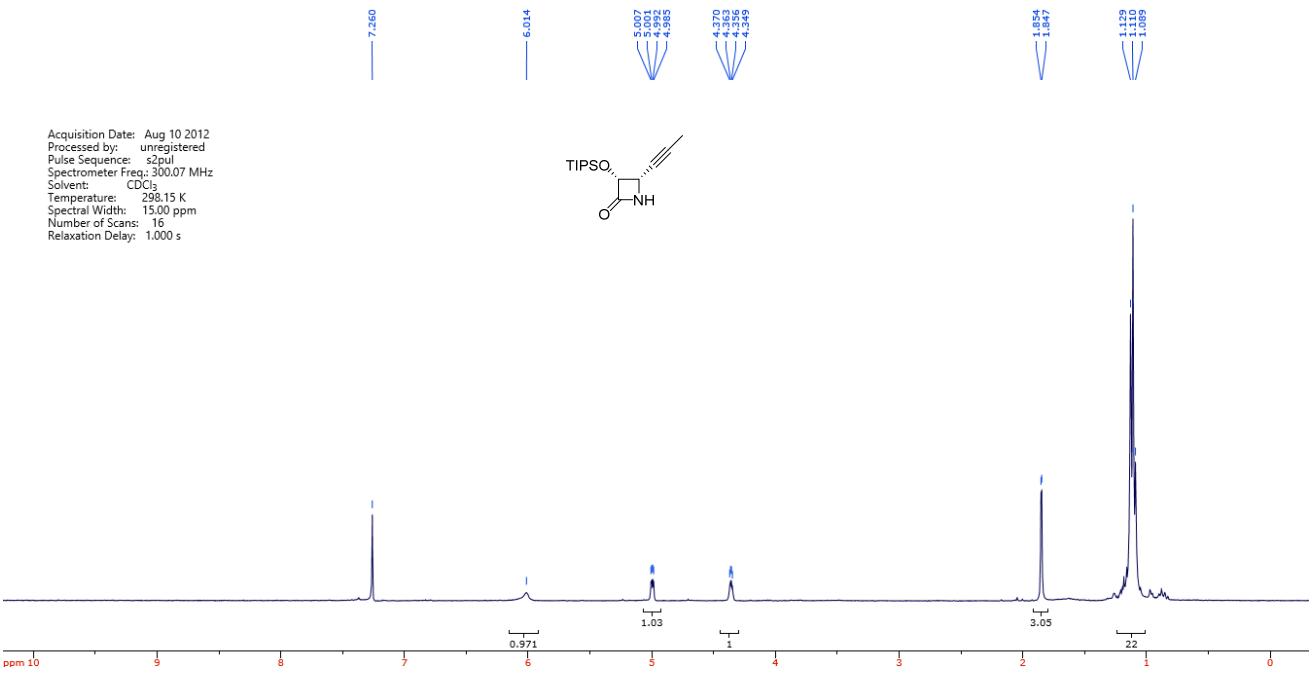

Figure S12. ^{1}H NMR spectrum of (+)-**16**

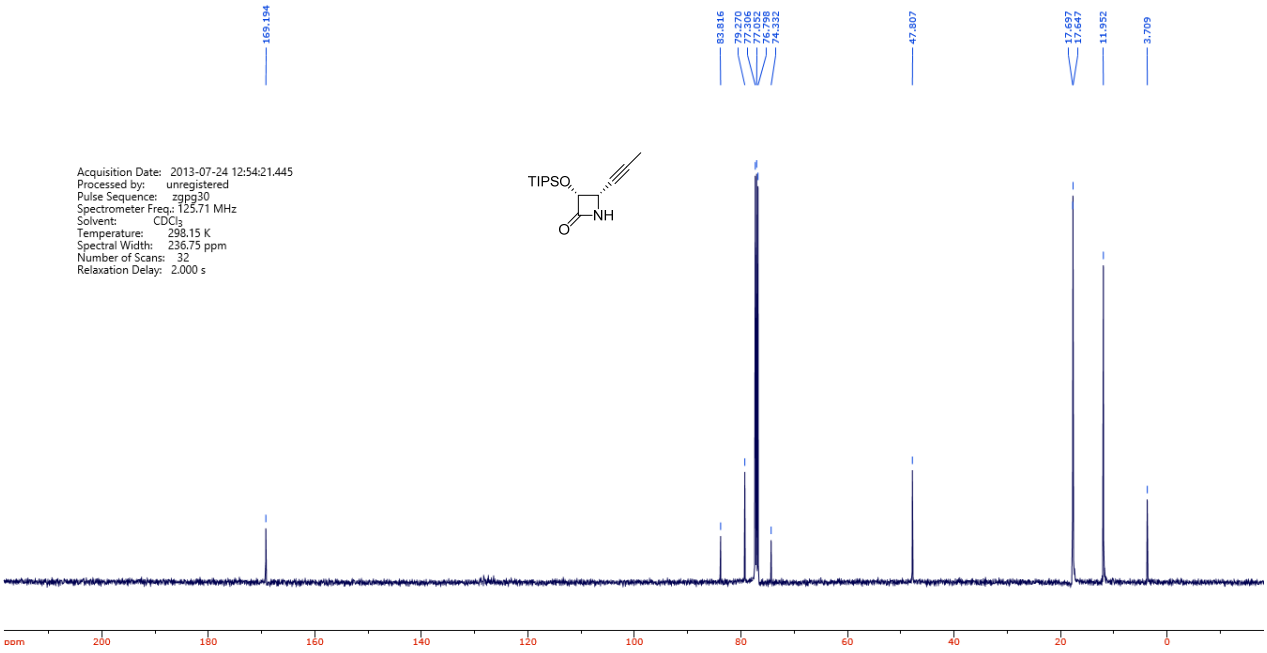

Figure S13. ^{13}C NMR spectrum of (+)-**16**

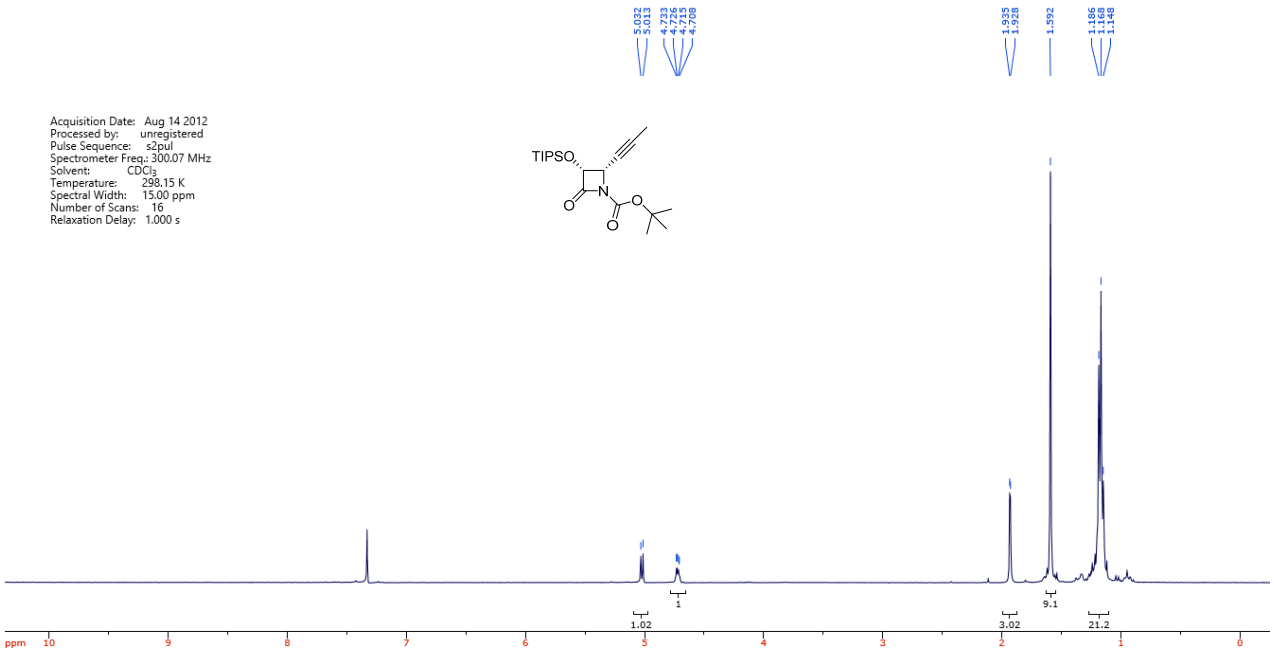

Figure S14. ^{1}H NMR spectrum of (+)**-5**

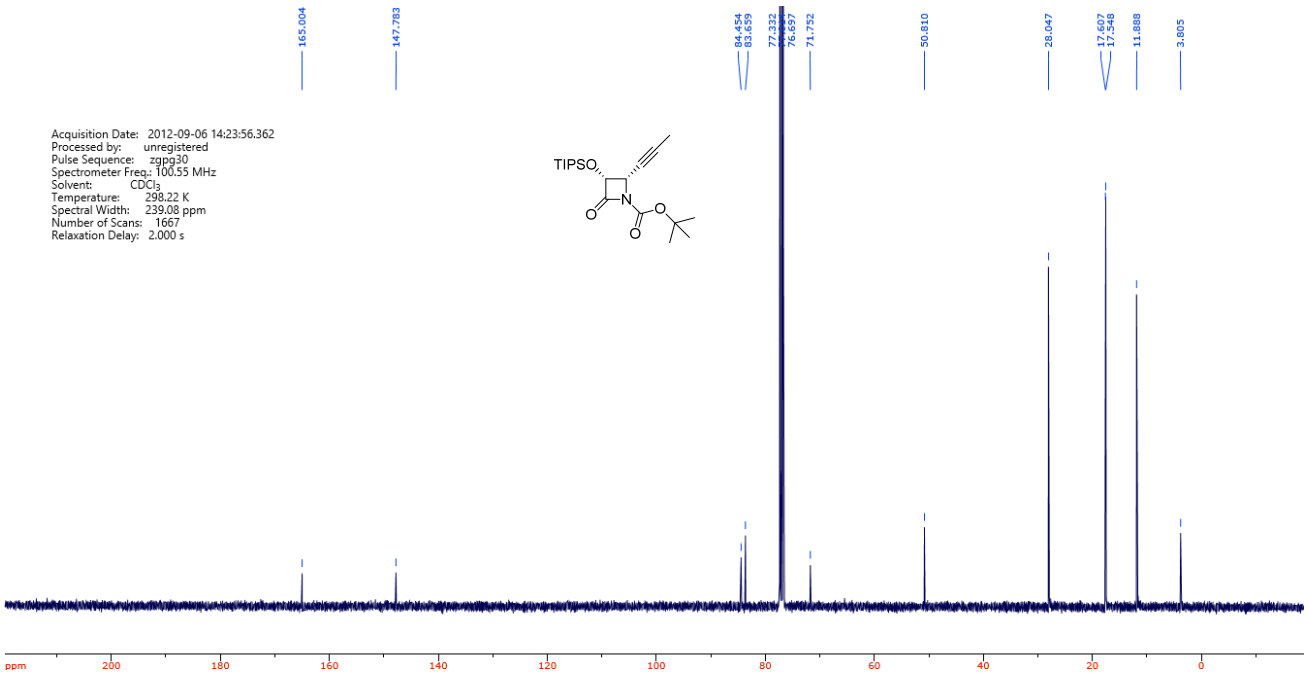

Figure S15. ^{13}C NMR spectrum of (+)**-5**

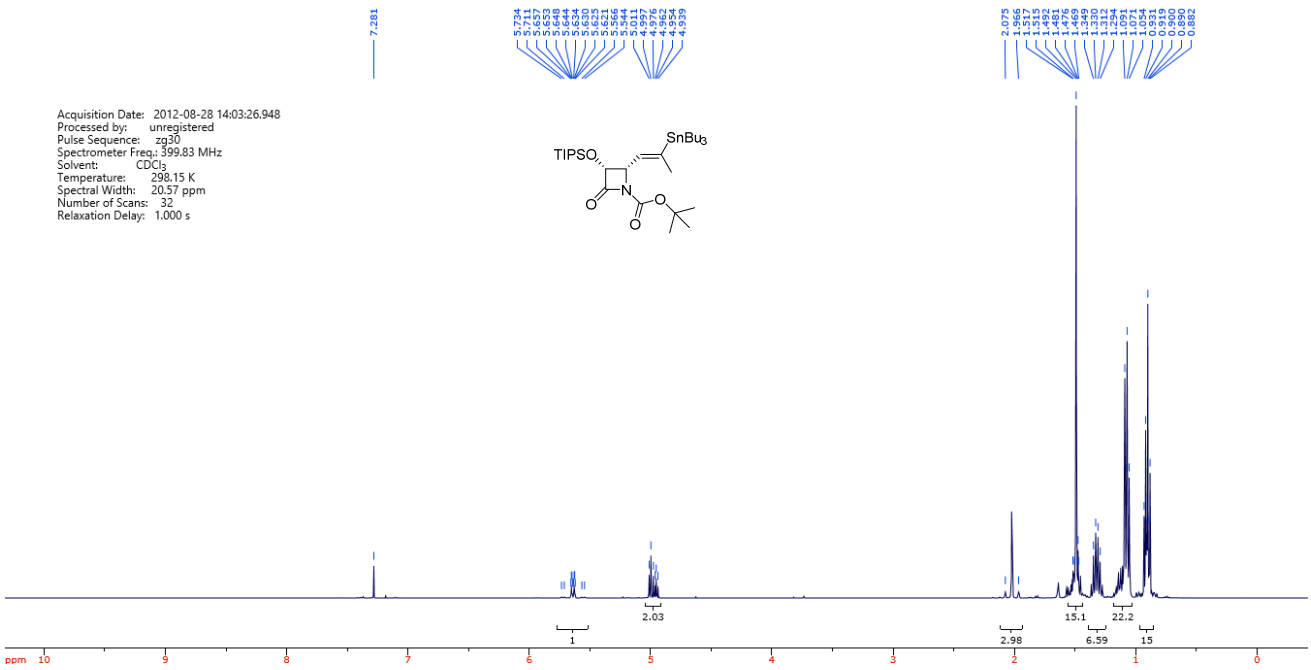

Figure S16. ^{1}H NMR spectrum of (+)**-4**

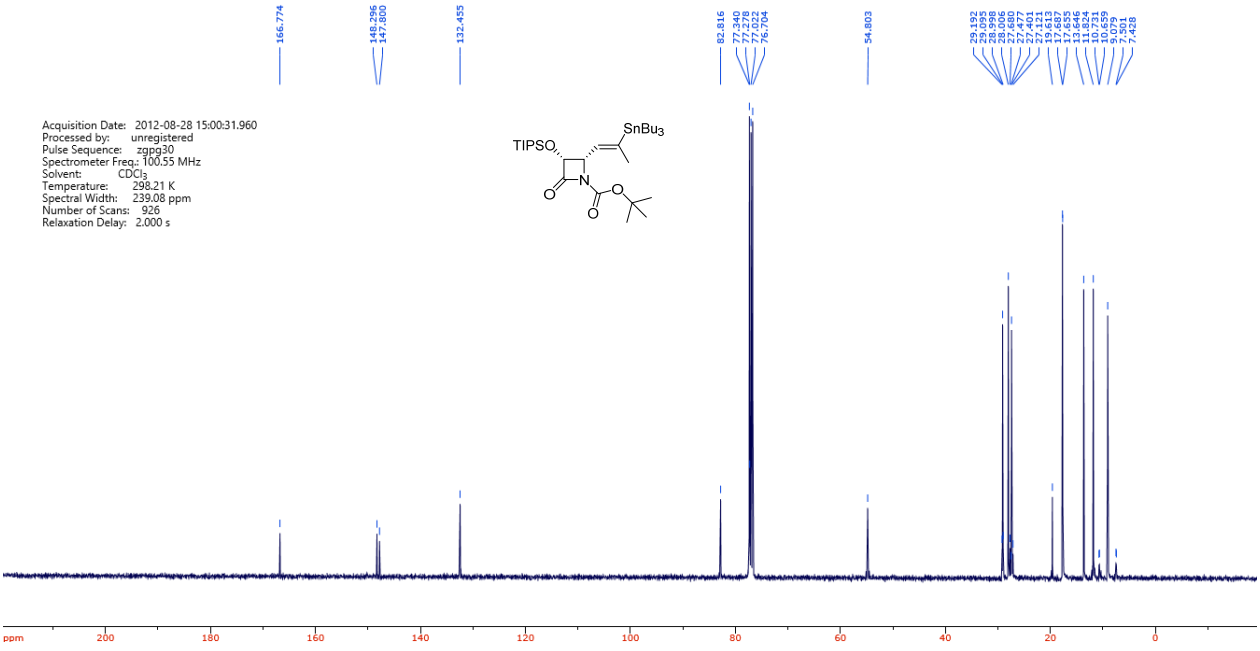

Figure S17. ^{13}C NMR spectrum of (+)**-4**

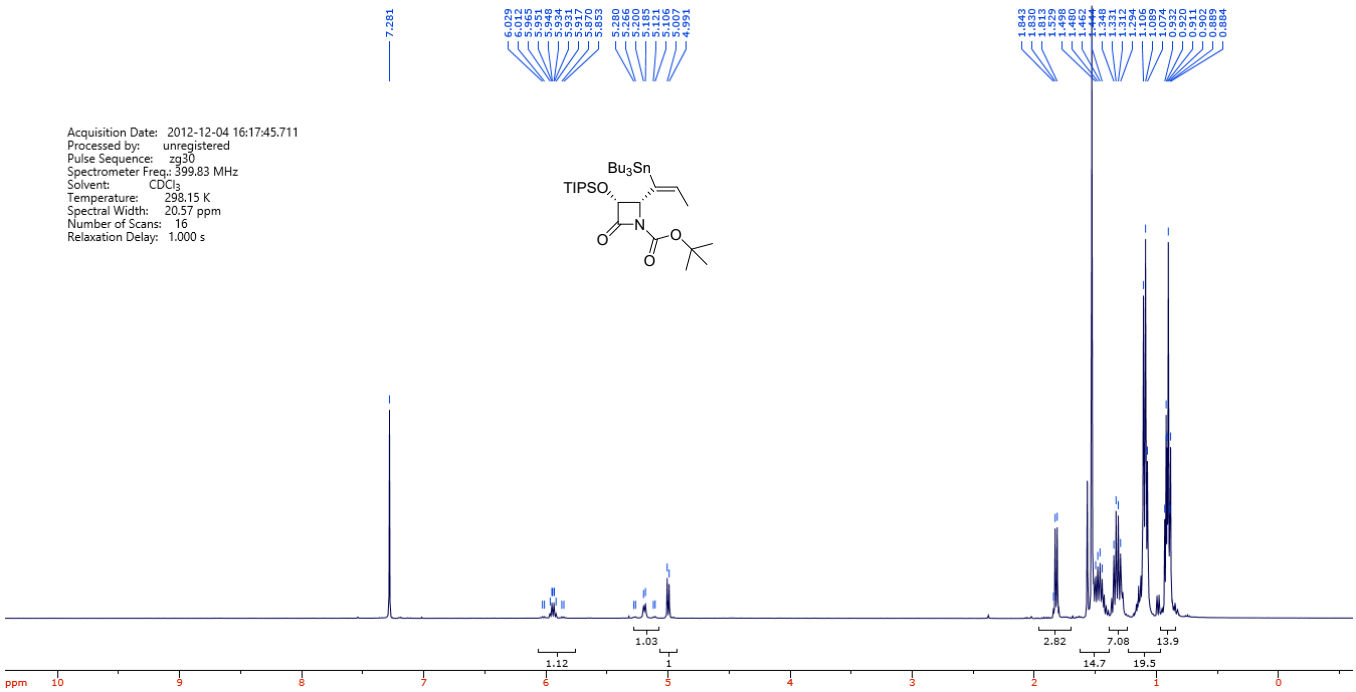

Figure S18. ^{1}H NMR spectrum of (+)-**17**

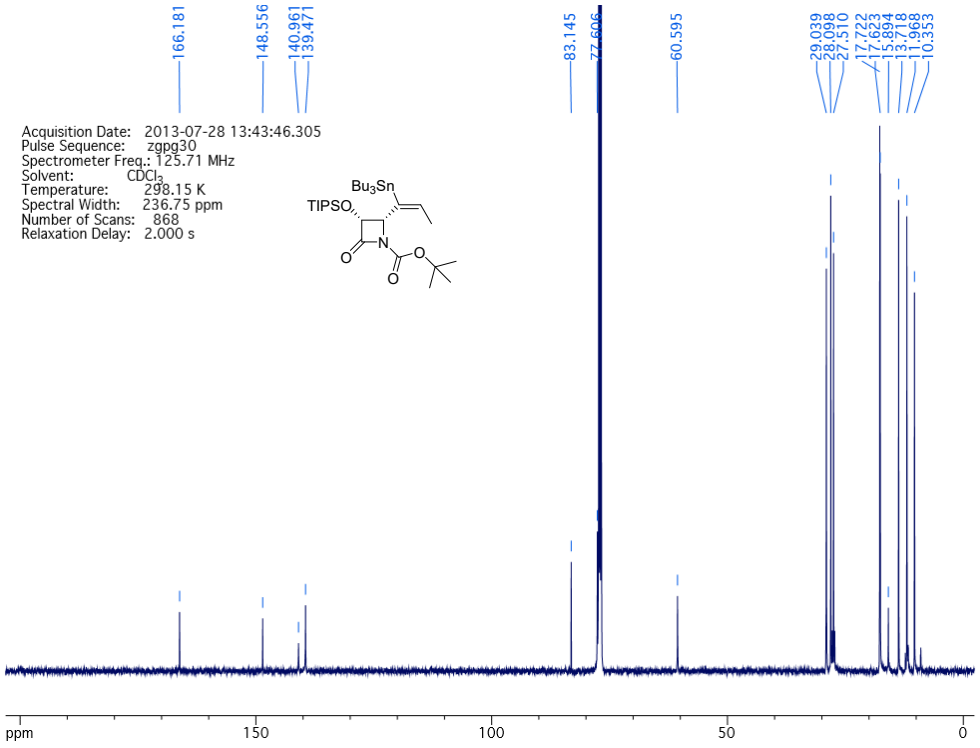

Figure S19. ^{13}C NMR spectrum of (+)-**17**

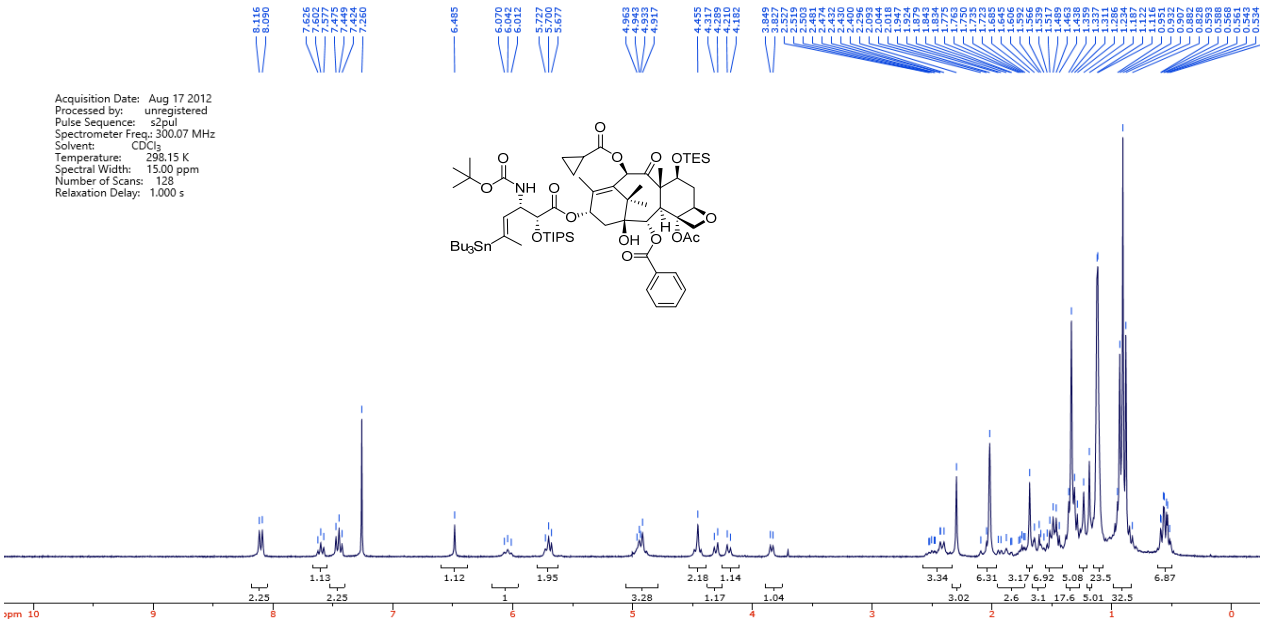

Figure S20. ^{1}H NMR spectrum of silyl-protected taxoid **18**

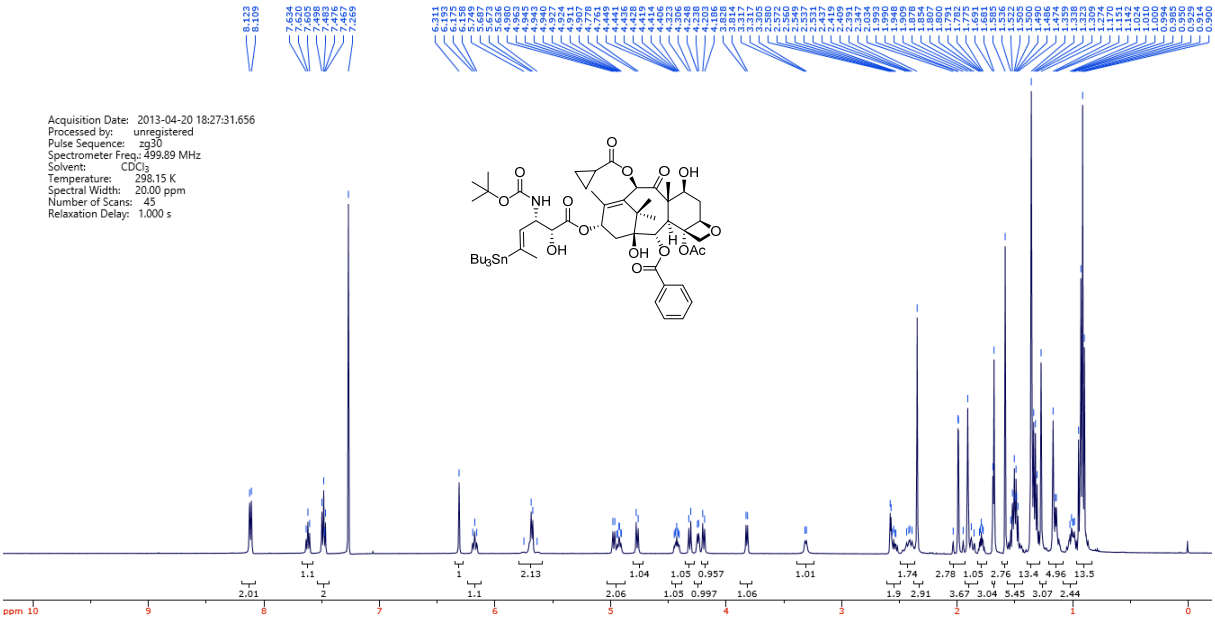

Figure S21. ^{1}H NMR Spectrum of **2**

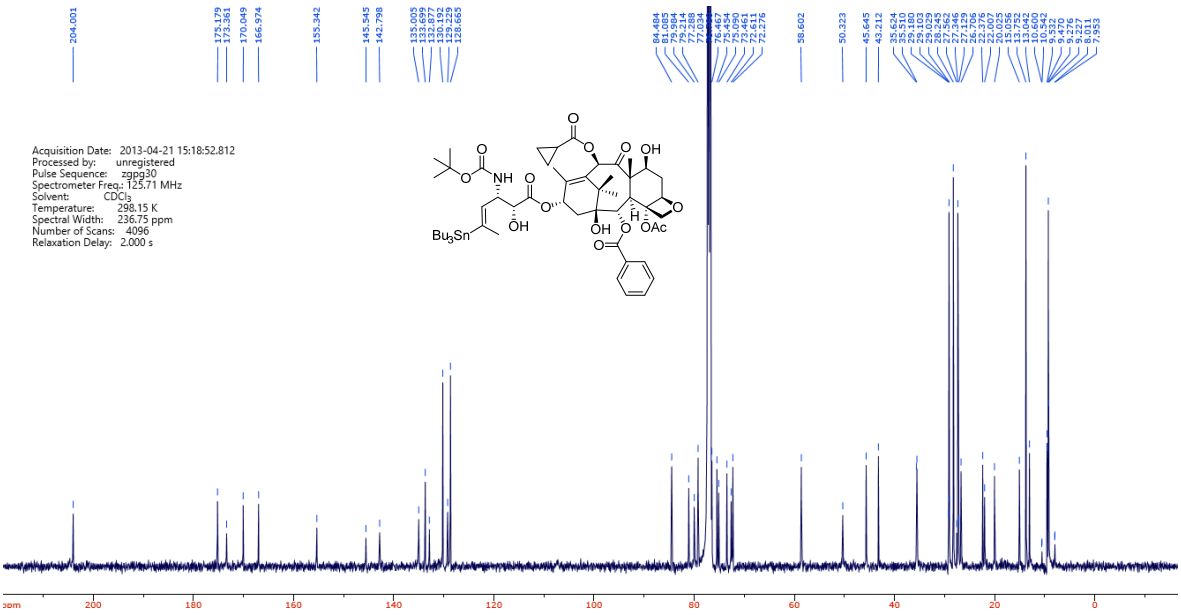

Figure S22. ^{13}C NMR Spectrum of **2**

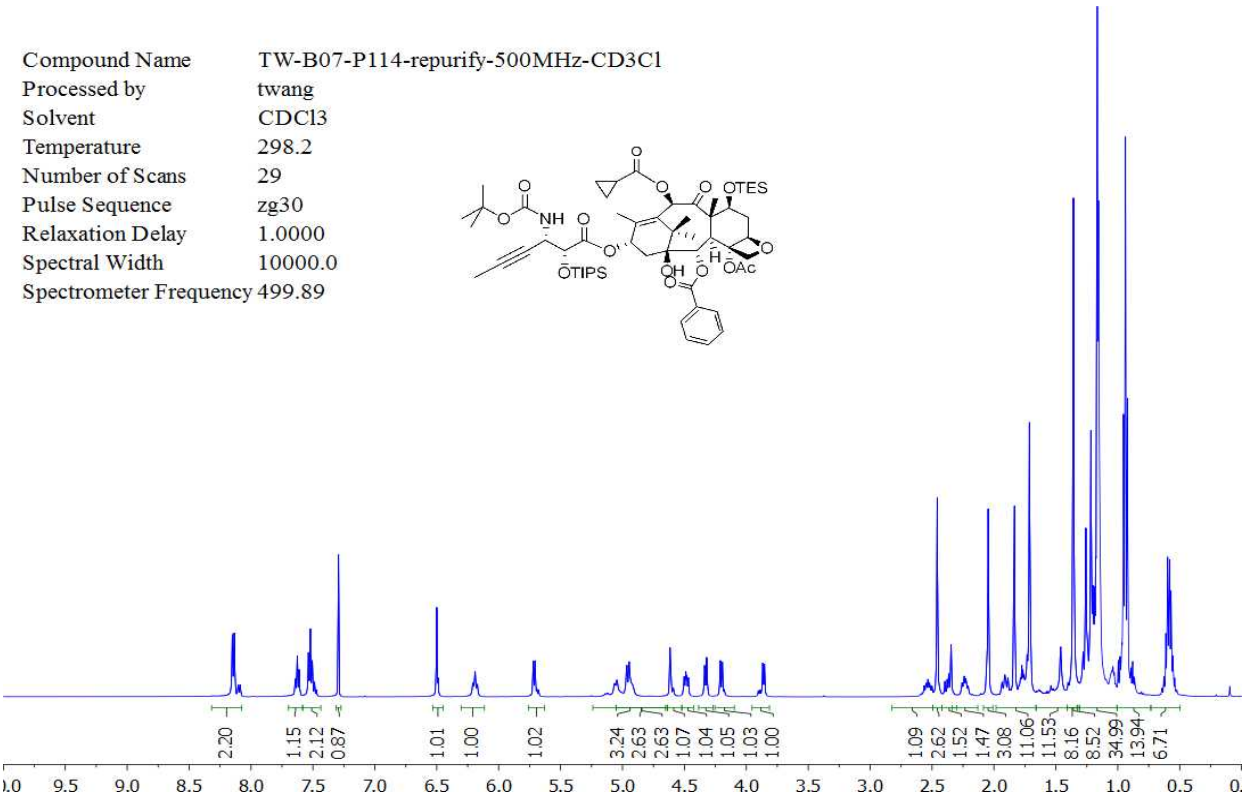

Figure S23. ^{1}H NMR spectrum of **23**

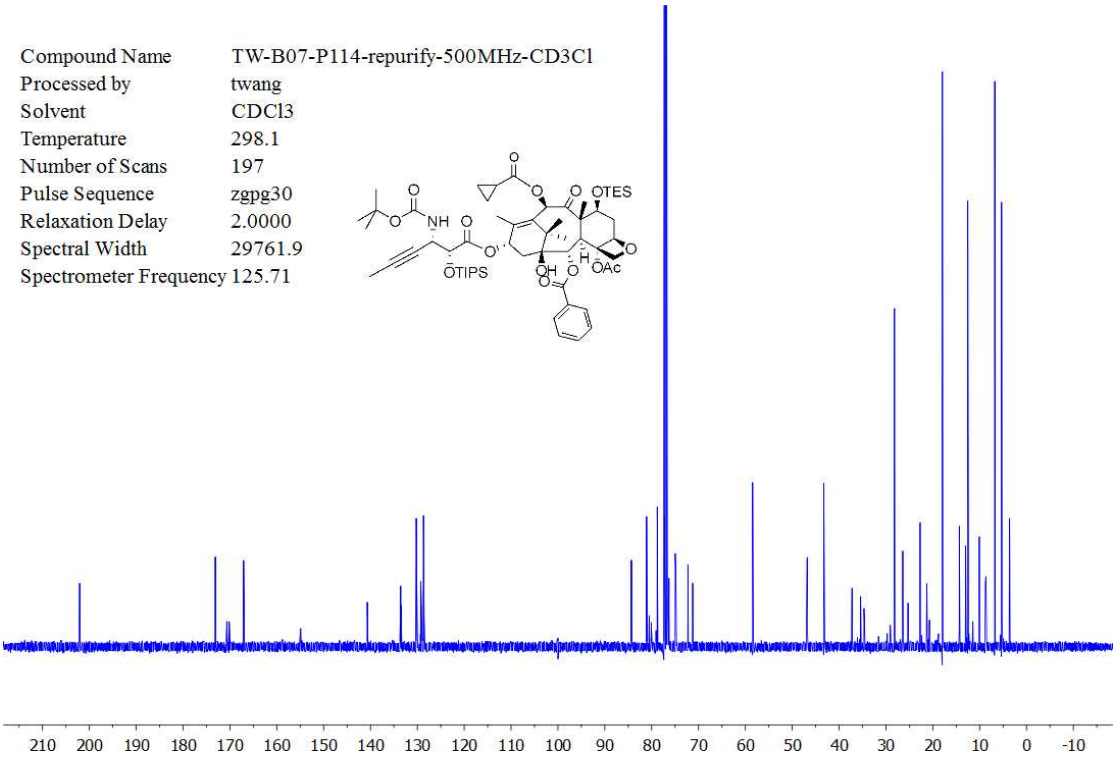

Figure S24. ^{13}C NMR spectrum of **23**

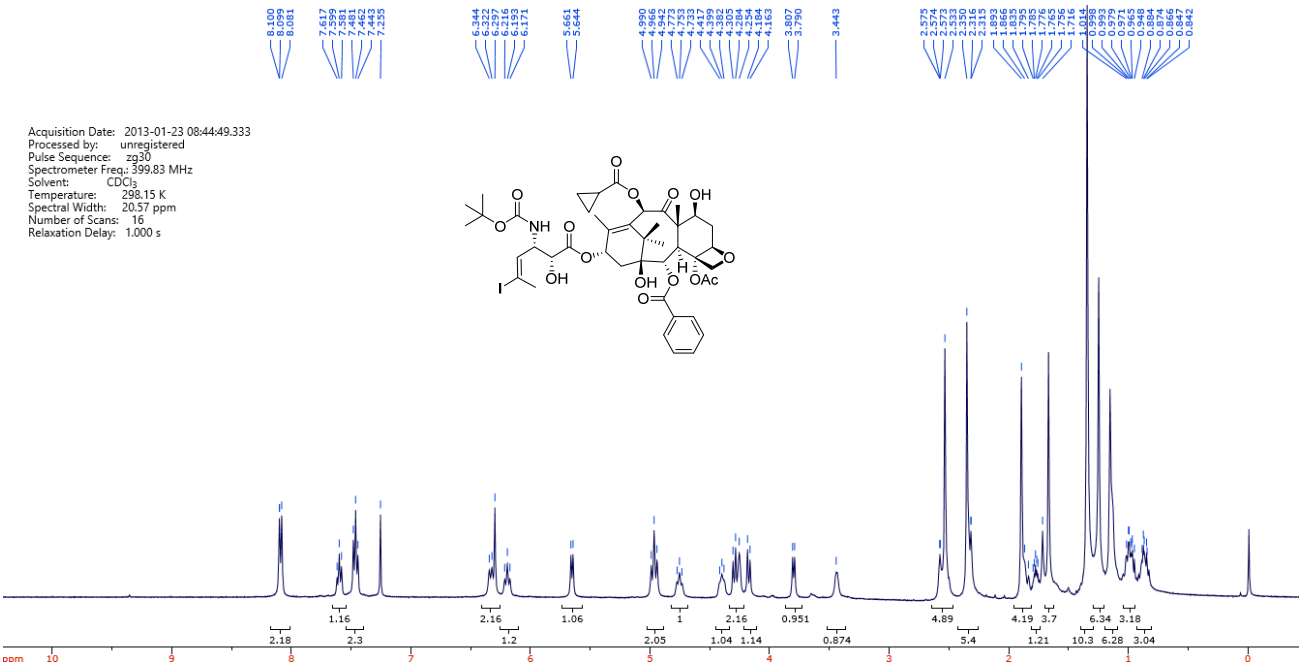

Figure S25. ^{1}H NMR spectrum of **19**

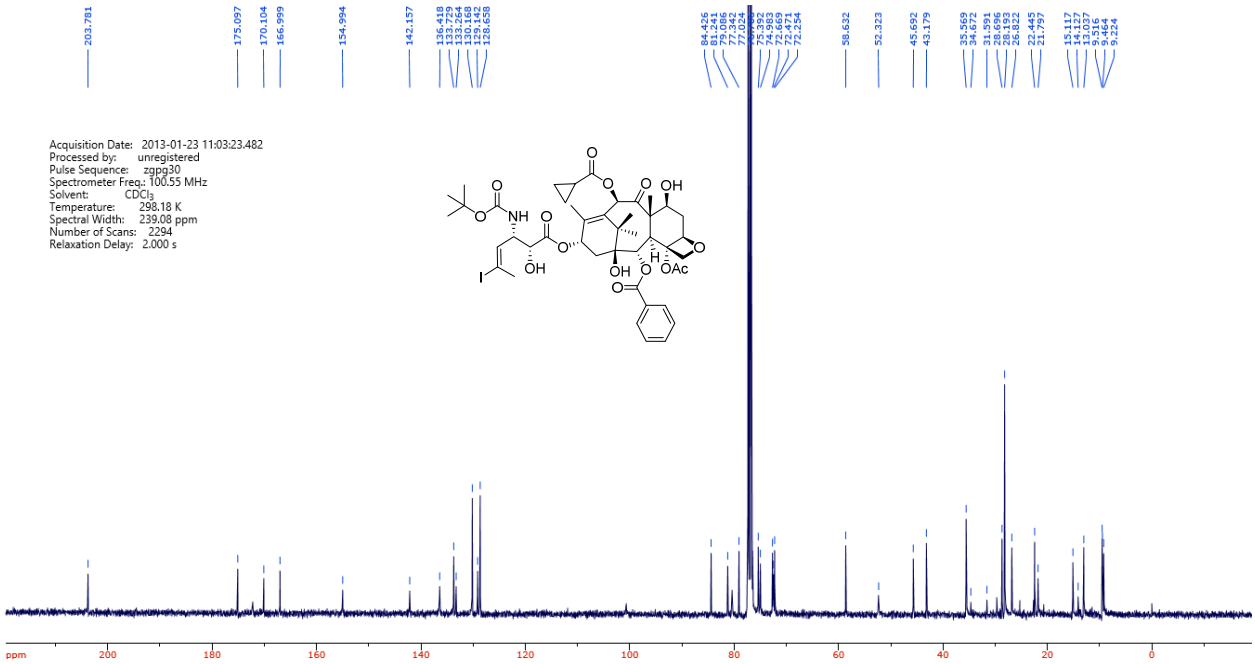

Figure S26. ^{13}C NMR spectrum of **19**

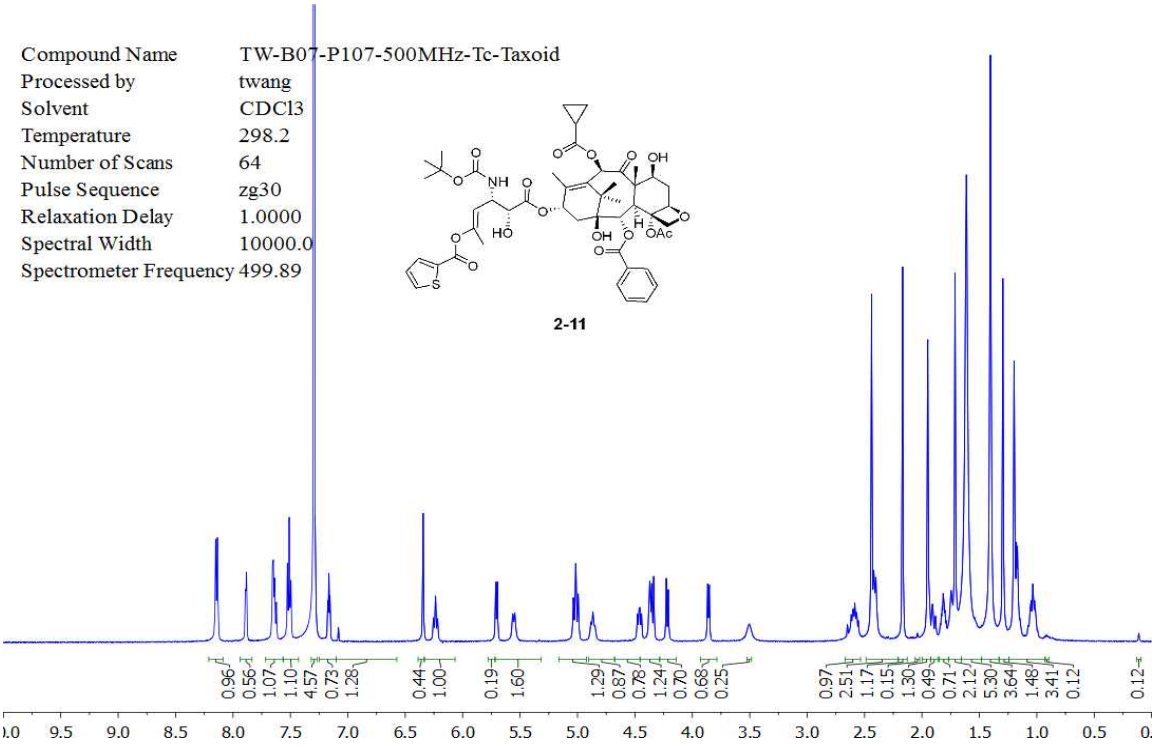

Figure S27. ^{1}H NMR spectrum of **20**

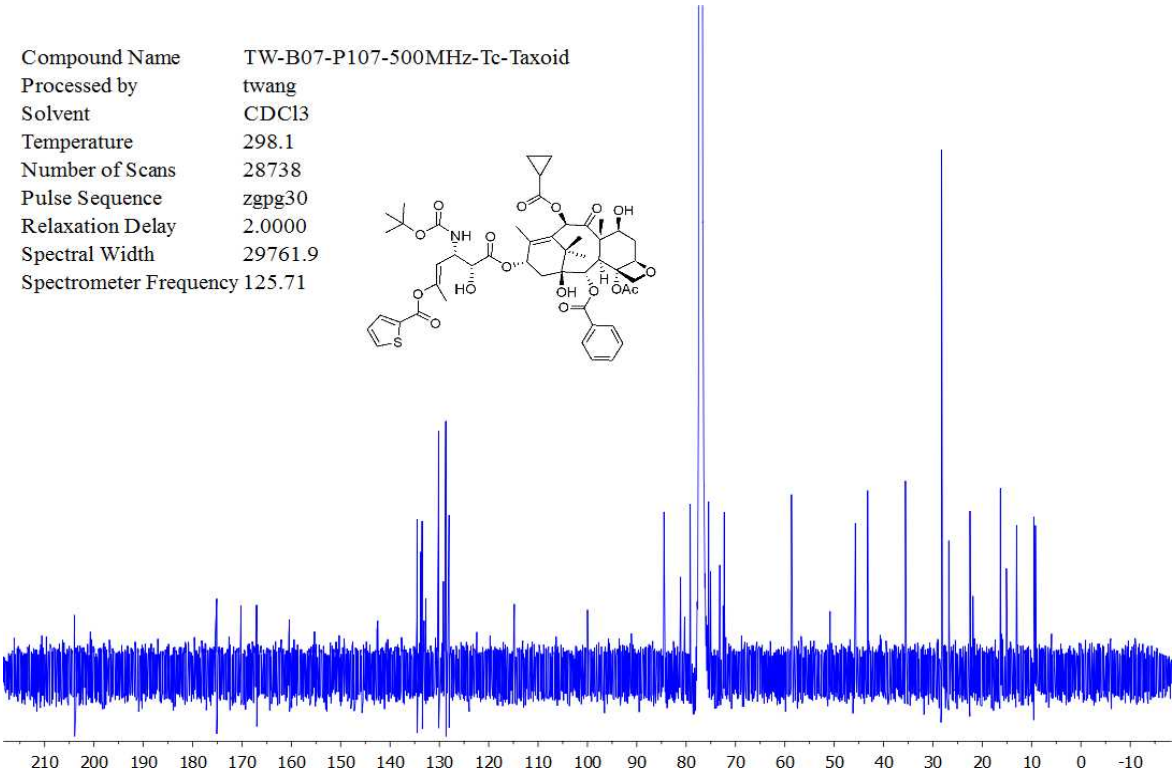

Figure S28. ^{13}C NMR spectrum of **20**

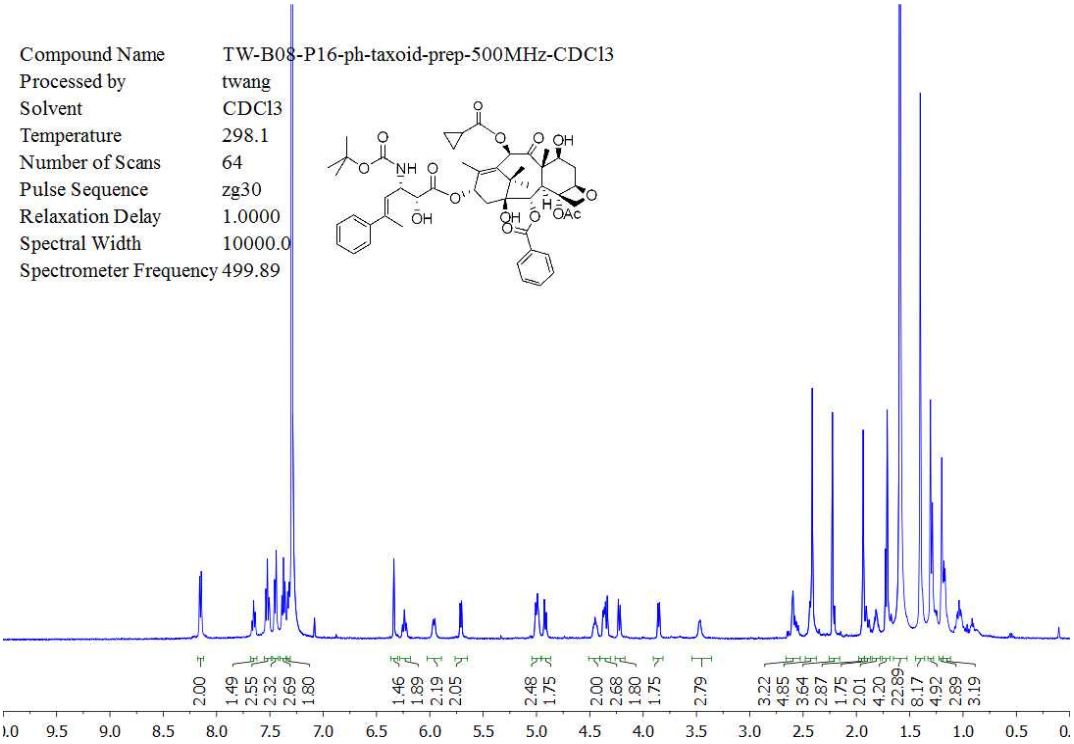

Figure S29. ^{1}H NMR spectrum of **21**

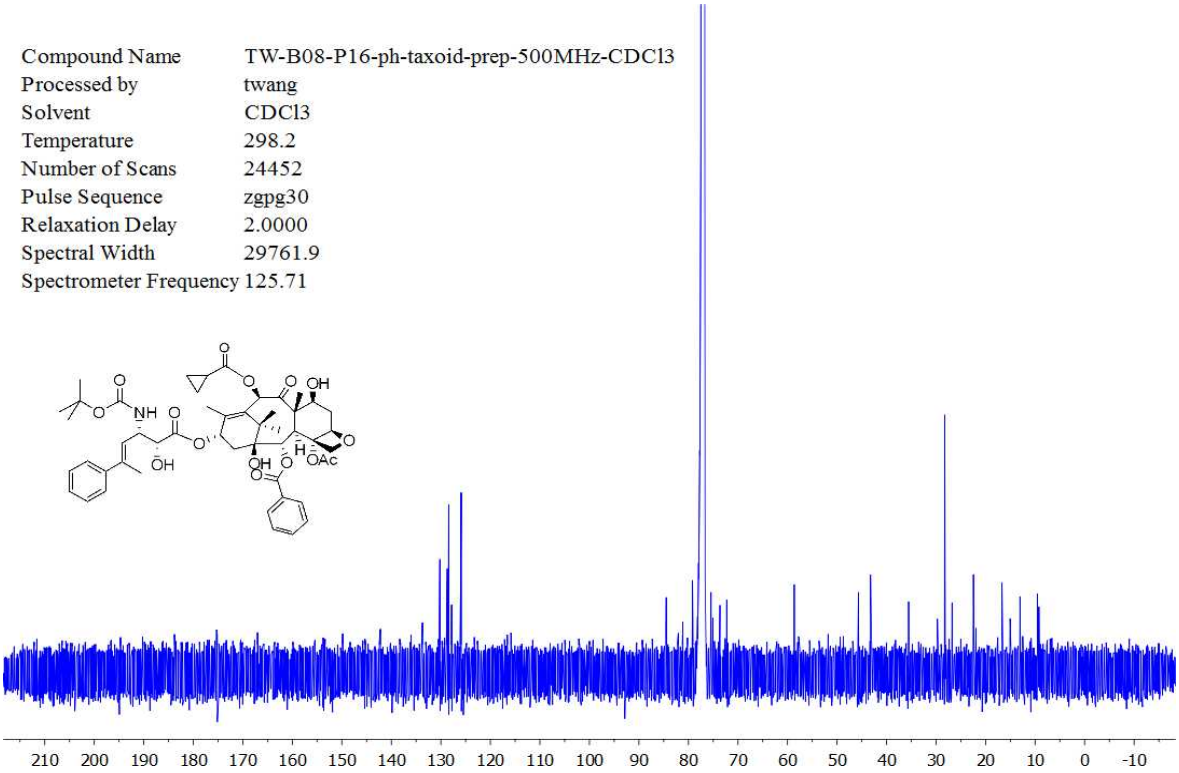

Figure S30. ^{13}C NMR spectrum of **21**

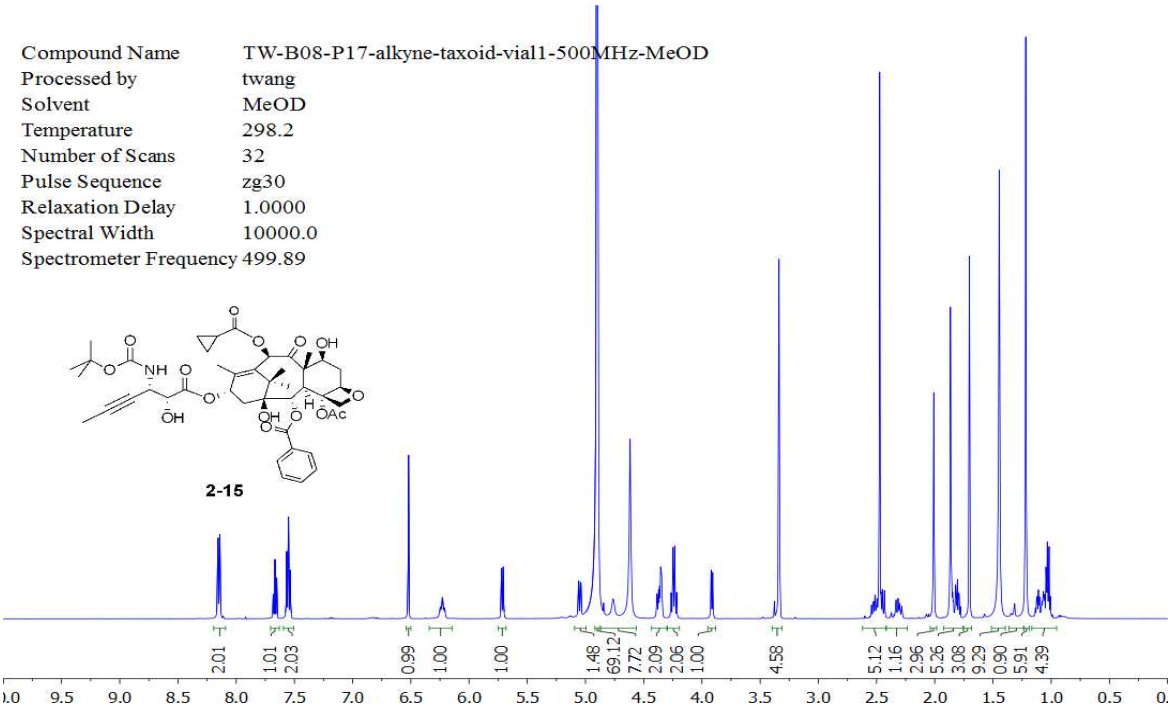

Figure S31. ^{1}H NMR spectrum of **22'**

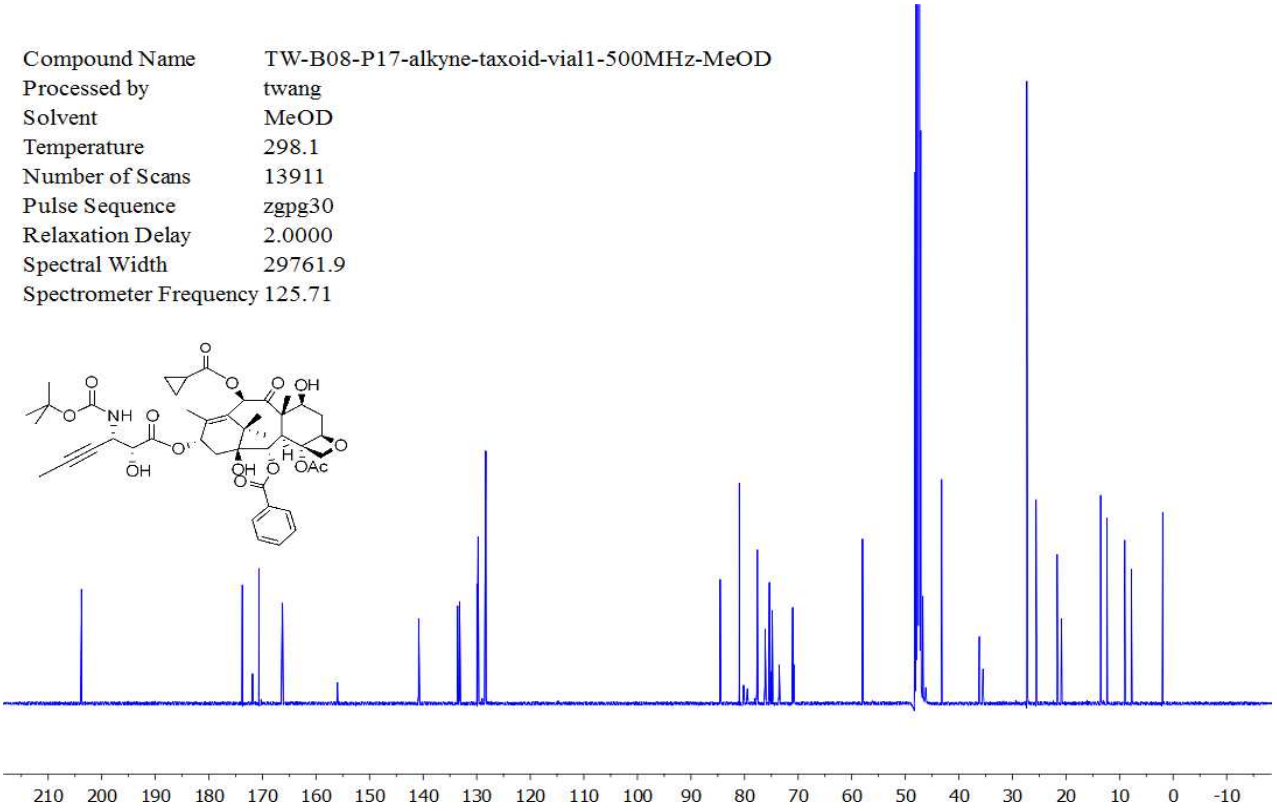

Figure S32. ^{13}C NMR spectrum of **22'**

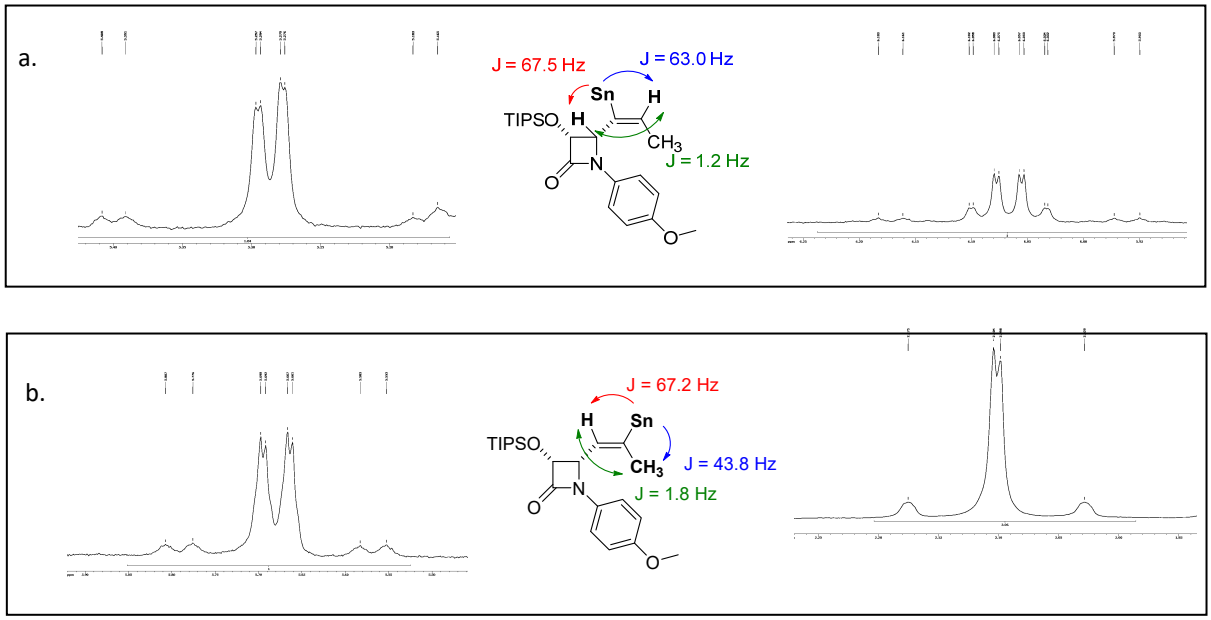

Figure S33. Assignment of regiochemistry for the regioisomers *a.)* **(±)-11** and *b.)* **(±)-10**, utilizing the splitting patterns due to the presence of NMR active Sn isotopes. Included in the figure are expansions of the ^{1}H NMR peaks used to make these assignments. The NMR excerpt to the left of the structure corresponds to the Sn-^{1}H J coupling denoted on the structure in red, while those on the right correspond to the Sn-^{1}H J values denoted in blue. The resolution of the satellite peaks is too low to distinguish between the ^{119}Sn and ^{117}Sn isotopes, so the Sn-^{1}H coupling constants were calculated from the apex of the broad satellite peaks. Additionally, allylic ^{1}H-^{1}H coupling can be seen between the two peaks, and the J value for this coupling in each structure is shown in green.

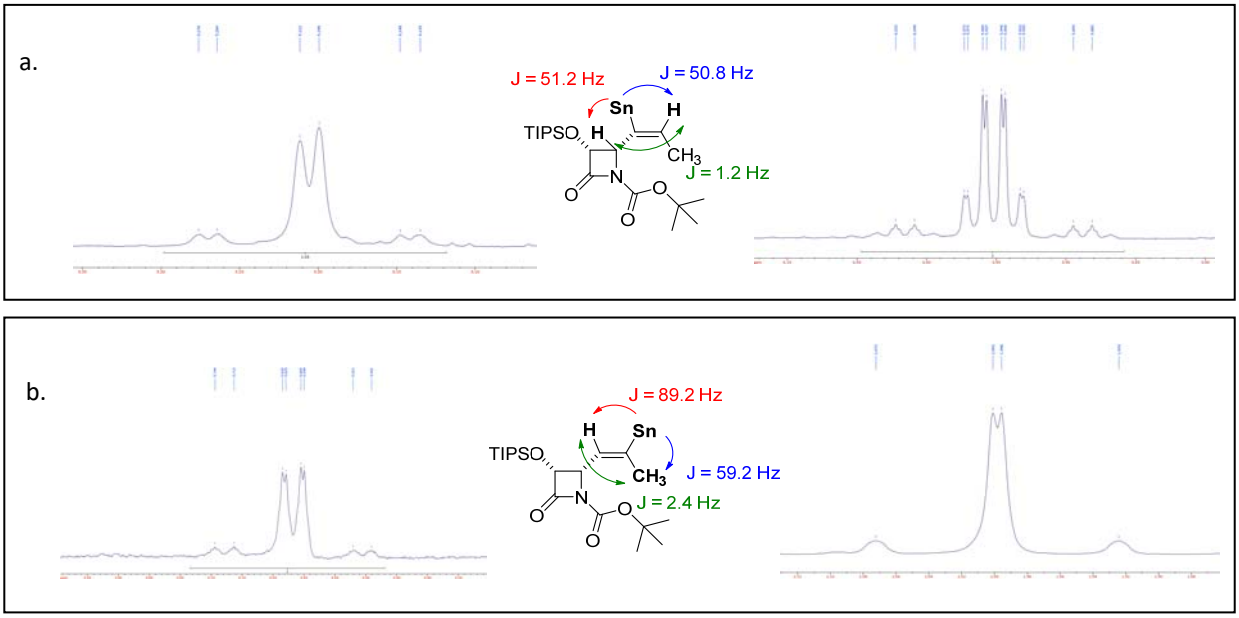

Figure S34. Assignment of regiochemistry for the regioisomers *a.)* **(+)-17** and *b.)* **(+)-4**, utilizing the splitting patterns due to the presence of NMR active Sn isotopes. Included in the figure are expansions of the ^{1}H NMR peaks used to make these assignments. The NMR excerpt to the left of the structure corresponds to the Sn-^{1}H J coupling denoted on the structure in red, while those on the right correspond to the Sn-^{1}H J values denoted in blue. The resolution of the satellite peaks is too low to distinguish between the ^{119}Sn and ^{117}Sn isotopes, so the Sn-^{1}H coupling constants were calculated from the apex of the broad satellite peaks. Additionally, allylic ^{1}H-^{1}H coupling can be seen between the two peaks, and the J value for this coupling in each structure is shown in green.

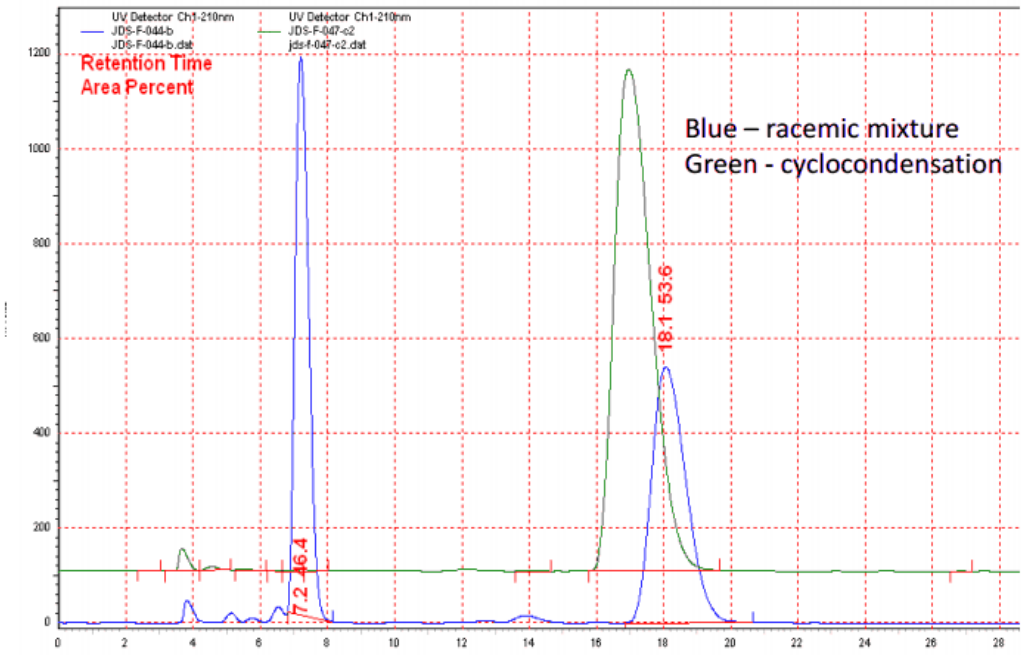

Figure S35. Chiral HPLC trace of racemic **(±)-9** (blue) and enantioenriched **(+)-9** (green), clearly demonstrating the enantioselectivity of the chiral ester enolate-imine cyclocondensation. Enantiomeric purity was assessed by normal phase HPLC on a Shimadzu LC-2010A with a chiracel OD-H column. The mobile phase was hexanes-IPA with an isocratic ratio of 98:2. The analyses were performed at a flow rate of 0.6 ml/min with the UV detector set at 210 nm.

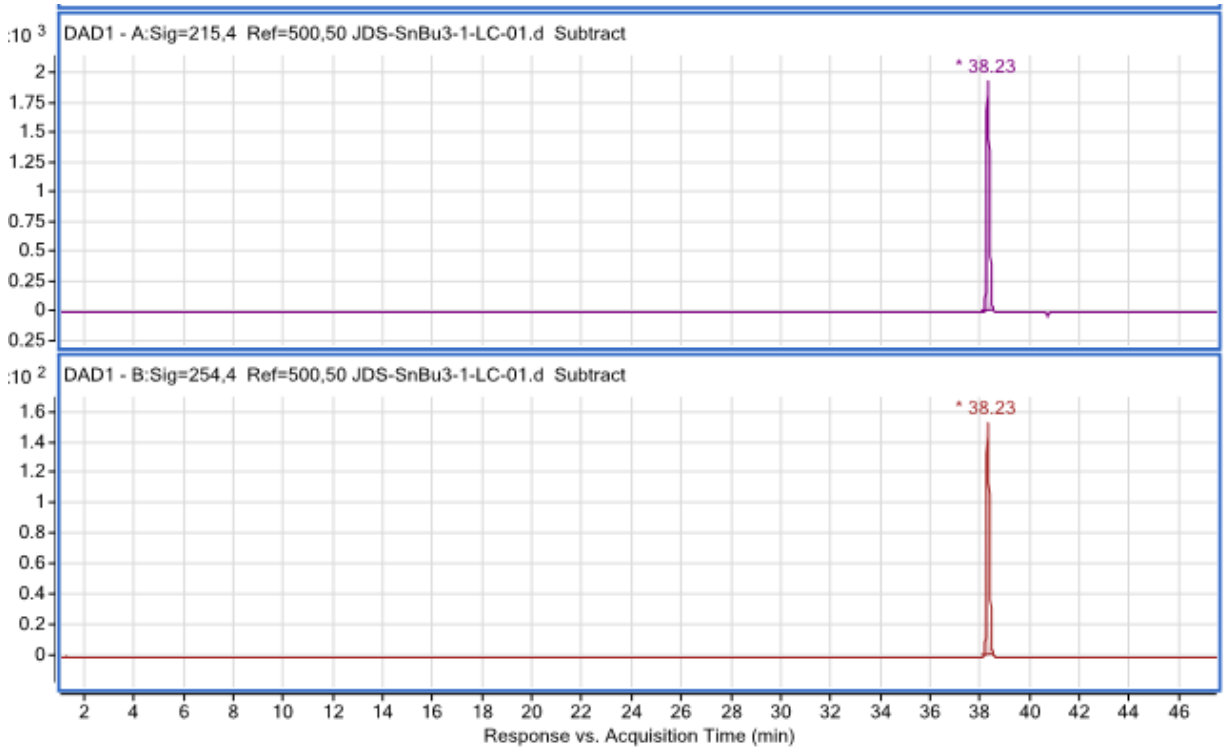

Figure S36. HPLC trace of **2**. Purity of **2** was analyzed using LC/HRMS with a Kinetex PFP column (100Å, 2.6µm, 100x2mm/mm) using background subtraction of pure methanol. The mobile phase was 10 mM aqueous ammonium acetate and MeOH. Analysis was performed at a flow rate of 0.4 mL/min using the following gradient: t=0–5 min: 60% MeOH; t=5–15 min: 60–65% MeOH; t=15–20 min: 65–70% MeOH; t=20–30 min: 70–75% MeOH; t=30–40 min: 75–95% MeOH; t=40–50 min: 95% MeOH. The UV detector was set for 215.4 and 254.4 nm.

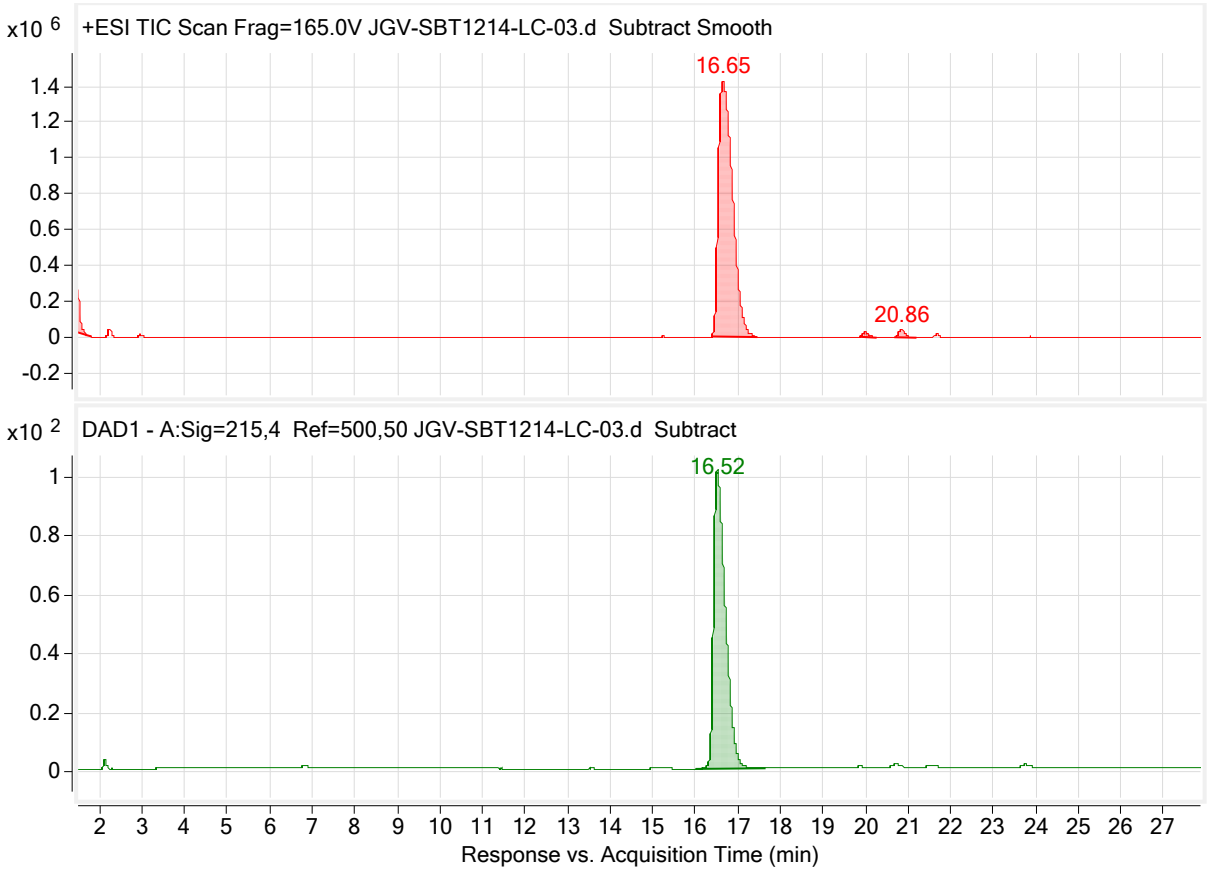

Figure S37. HPLC trace of **1**, synthesized by known literature method.[1] Purity of **1** was analyzed using LC-UV-TOF (HRMS) with a Kinetex PFP column (100Å, 2.6µm, 100x2mm/mm) using background subtraction of pure methanol. The mobile phase was 10 mM aqueous ammonium acetate and MeOH. Analysis was performed at a flow rate of 0.4 mL/min using the following gradient: t=0–5 min: 60% MeOH; t=5–15 min: 60–65% MeOH; t=15–20 min: 65–70% MeOH; t=20–30 min: 70–75% MeOH; t=30–40 min: 75–95% MeOH; t=40–50 min: 95% MeOH. The UV detector was set for 215.4 and 254.4 nm.

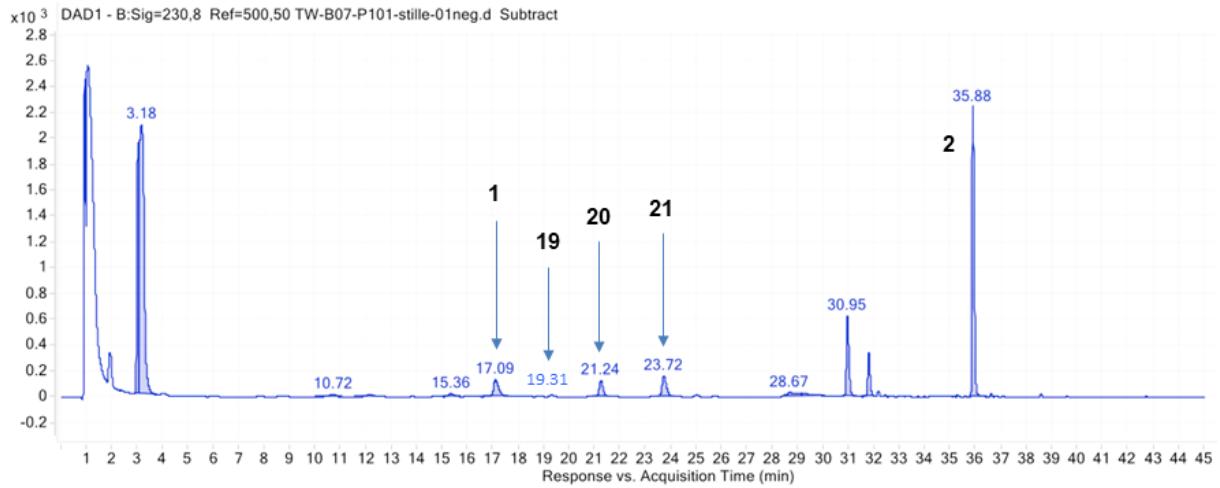

Figure S38. HPLC-UV chromatogram of the Stille coupling reaction mixture using CH_3I (1 equiv.) at 220 nm using an Agilent LC-UV-TOF (HRMS) instrument with a Kinetex PFP column (100 Å, 2.6 µm, 150x2.1 mm/mm) at 30 °C using background subtraction of pure methanol. The mobile phase was 10 mM aqueous ammonium acetate and MeOH. Analysis was performed at a flow rate of 0.38 mL/min using the following gradient: t=1-10 min, MeOH 60%; t=10-15 min, MeOH 60-70%; t=15-25 min, MeOH t=70-75%, t=25-35 min, MeOH t=75-95 %; t=35-45 min, 95-96.5%; t=45-48 min, MeOH 96.5-60%. **Note:** The side product eluted at 30.95 min was not a taxoid based on the fragmentation patterns as well as higher molecular weight in its mass spectrum.

.

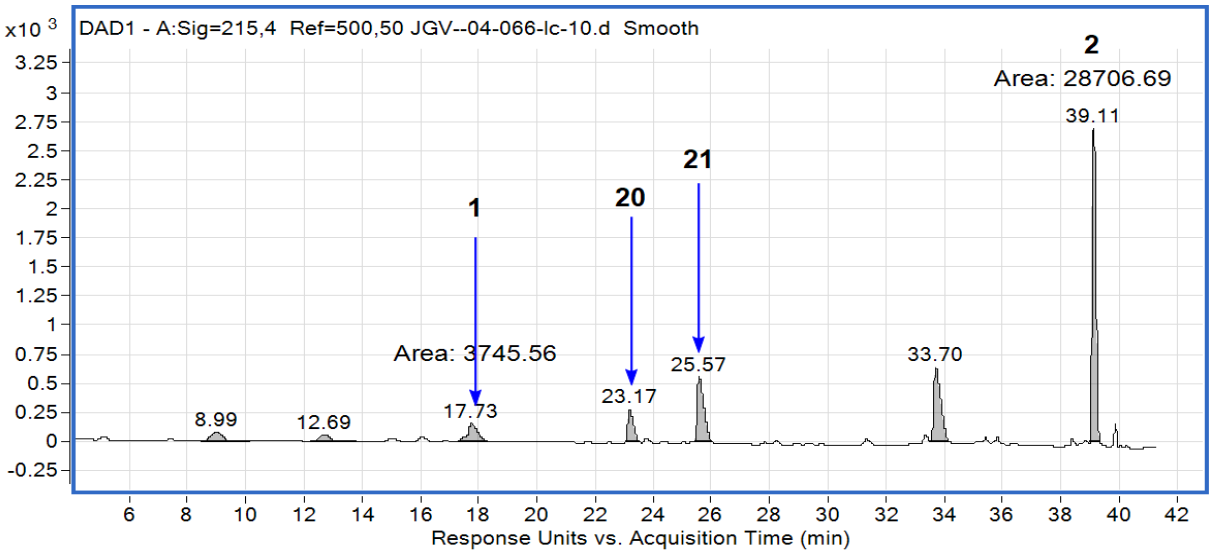

Figure S39. HPLC-UV chromatogram of the rapid Stille coupling reaction mixture using CH_3I (0.1 equiv) at 215 nm using an Agilent LC-UV-TOF (HRMS) instrument with a Kinetex PFP column (100 Å, 2.6 µm, 100x2 mm/mm) using background subtraction of pure methanol. The mobile phase was 10 mM aqueous ammonium acetate and MeOH. Analysis was performed at a flow rate of 0.4 mL/min using the following gradient: t=0-5 min: 60% MeOH; t=5-15 min: 60-65% MeOH; t=15-20 min: 65-70% MeOH; t=20-30 min: 70- 75% MeOH; t=30-40 min: 75-95% MeOH; t=40-50 min: 95% MeOH.